CNNM2, Encoding a Basolateral Protein Required for Renal Mg^{2+} Handling, Is Mutated in Dominant Hypomagnesemia

Marchel Stuiver,[1,2] Sergio Lainez,[3] Constanze Will,[1,2] Sara Terryn,[4] Dorothee Günzel,[5] Huguette Debaix,[4] Kerstin Sommer,[1,2] Kathrin Kopplin,[1,2] Julia Thumfart,[1,2] Nicole B. Kampik,[6] Uwe Querfeld,[1,2] Thomas E. Willnow,[7] Vladimír Němec,[8] Carsten A. Wagner,[6] Joost G. Hoenderop,[3] Olivier Devuyst,[4,6] Nine V.A.M. Knoers,[9] René J. Bindels,[3] Iwan C. Meij,[7,10] and Dominik Müller[1,2,10,*]

Familial hypomagnesemia is a rare human disorder caused by renal or intestinal magnesium (Mg^{2+}) wasting, which may lead to symptoms of Mg^{2+} depletion such as tetany, seizures, and cardiac arrhythmias. Our knowledge of the physiology of Mg^{2+} (re)absorption, particularly the luminal uptake of Mg^{2+} along the nephron, has benefitted from positional cloning approaches in families with Mg^{2+} reabsorption disorders; however, basolateral Mg^{2+} transport and its regulation are still poorly understood. Here, by using a candidate screening approach, we identified *CNNM2* as a gene involved in renal Mg^{2+} handling in patients of two unrelated families with unexplained dominant hypomagnesemia. In the kidney, CNNM2 was predominantly found along the basolateral membrane of distal tubular segments involved in Mg^{2+} reabsorption. The basolateral localization of endogenous and recombinant CNNM2 was confirmed in epithelial kidney cell lines. Electrophysiological analysis showed that CNNM2 mediated Mg^{2+}-sensitive Na^{+} currents that were significantly diminished in mutant protein and were blocked by increased extracellular Mg^{2+} concentrations. Our data support the findings of a recent genome-wide association study showing the *CNNM2* locus to be associated with serum Mg^{2+} concentrations. The mutations found in *CNNM2*, its observed sensitivity to extracellular Mg^{2+}, and its basolateral localization signify a critical role for CNNM2 in epithelial Mg^{2+} transport.

Introduction

Magnesium (Mg^{2+}) plays a crucial role in many biological processes such as enzyme and muscular function and neuronal transmission. In adults, the normal serum Mg^{2+} concentration ranges from 0.7 to 1.2 mmol/l. Low levels of serum Mg^{2+} may be asymptomatic and go unnoticed for a long time but may also cause tetany, convulsions, cardiac arrhythmias, and various metabolic abnormalities.

Mg^{2+} homeostasis is primarily regulated by intestinal absorption and renal reabsorption involving a combination of paracellular and transcellular epithelial transport pathways.[1] As a result of screening of familial cases of hypomagnesemia, several genes involved in renal Mg^{2+} handling in both the paracellular and the transcellular pathways have been discovered. For example, the tight junction proteins claudin-16 (CLDN16 [MIM 603959]) and claudin-19 (CLDN19 [MIM 610036]) are mutated in recessive familial hypomagnesemia with hypercalciuria and nephrocalcinosis (FHHNC, [MIM 248250, 248190]).[2,3] They are primarily involved in the paracellular pathway, either, as initially suggested, by forming a selective permeability for Mg^{2+} and Ca^{2+} or, as more recently proposed, by altering the driving force for reabsorption of divalent cations by selective back-leakage of Na^{+} or by altering Cl^{-} secretion.[2,4–6] A key protein in the transcellular pathway is the epithelial Mg^{2+} channel TRPM6 (MIM 607009), which, when mutated, causes recessive hypomagnesemia with secondary hypocalcemia (HSH [MIM 602014]).[7,8] Other genes mutated in human renal Mg^{2+} wasting disorders, such as *FXYD2* (MIM 601814, associated with dominant renal hypomagnesemia [MIM 154020]), *EGF* (MIM 131530, associated with recessive renal hypomagnesemia [MIM 611718]), *KCNA1* (MIM 176260, associated with dominant myokymia with hypomagnesemia [MIM 160120]), and *HNF1B* (MIM 189907, associated with dominant renal cysts and diabetes syndrome [MIM 137920]) are also thought to be involved in transcellular Mg^{2+} reabsorption.[9–12] Whereas the apical entry pathway for Mg^{2+} in the renal distal convoluted tubule (DCT) formed by TRPM6 is relatively well characterized,[13] the molecular identity of basolateral extrusion mechanisms for Mg^{2+} remain elusive.

We recently generated mice lacking claudin-16 to gain insights into pathways relevant for renal Ca^{2+} and Mg^{2+} handling.[14] *Cldn16*-deficient mice displayed renal Ca^{2+} and Mg^{2+} wasting as well as alterations in the renal

[1]Department of Pediatric Nephrology, Charité Universitätsmedizin Berlin, 13353 Berlin, Germany; [2]Center for Cardiovascular Research, Charité Universitätsmedizin Berlin, 10115 Berlin, Germany; [3]Department of Physiology, Radboud University Nijmegen Medical Centre, 6500 HB Nijmegen, The Netherlands; [4]Division of Nephrology, Université Catholique de Louvain Medical School, 1200 Brussels, Belgium; [5]Institute of Clinical Physiology, Charité Universitätsmedizin Berlin, 12200 Berlin, Germany; [6]Institute of Physiology and Zurich Center for Integrative Human Physiology, University of Zurich, 8057 Zurich, Switzerland; [7]Max Delbrück Center for Molecular Medicine, 13092 Berlin, Germany; [8]Department of Pediatrics, Pardubice Regional Hospital, 532 03 Pardubice, Czech Republic; [9]Department of Medical Genetics, University Medical Centre Utrecht, 3508 AB Utrecht, The Netherlands
[10]These authors contributed equally to this work
*Correspondence: dominik.mueller@charite.de
DOI 10.1016/j.ajhg.2011.02.005.

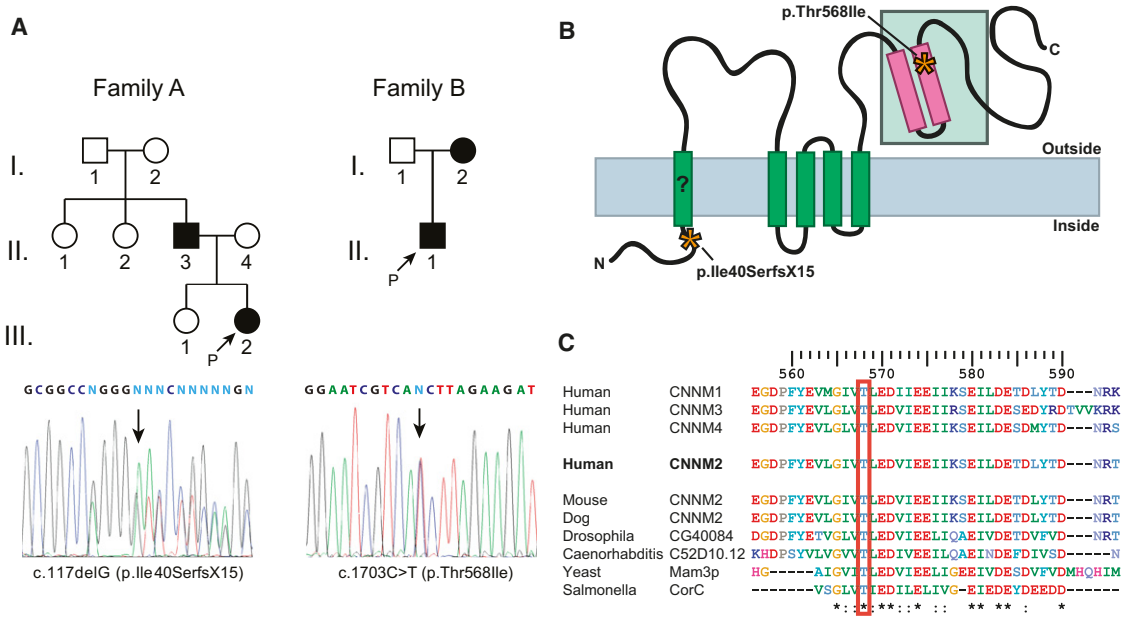

Figure 1. Pedigrees of Families and *CNNM2* Mutations
(A) Pedigrees of families A (left) and B (right) and partial electropherograms of *CNNM2* of the index patients. Filled symbols represent affected individuals and index patients are indicated with a "P" and arrow. In the electropherograms, the mutations are indicated by an arrow and the nucleotide changes and resulting effect on the protein are shown.
(B) Localization of the mutations in the predicted secondary structure of CNNM2. The predicted transmembrane domains are indicated in green and the CBS domains in pink. The ancient conserved domain is boxed and the mutations are indicated with an asterisk.
(C) Conservation of human CNNM2 Thr568 in CNNM family members and in orthologs from mammals to bacteria. The amino acid sequence of human CNNM2 (in bold) is aligned with its three human family members and six orthologs around Thr568 (boxed in red). The upper ruler refers to the human CNNM2 amino acid positions. Conservation is shown below the sequences, following ClustalW convention (asterisk, invariant; colon, highly similar).

transcriptome as shown by microarray analysis. Some of the differentially expressed mRNAs encode proteins well known for their involvement in renal Ca^{2+} and Mg^{2+} handling, such as the epithelial Ca^{2+} and Mg^{2+} entry channels TRPV5 and TRPM6 and the basolateral Na^{+}/Ca^{2+} exchanger. In addition, we identified other, not well-characterized upregulated transcripts, one of which encodes CNNM2 (previously known as ACDP2).[14] The *Cnnm2* transcript caught our interest because it has been shown to be upregulated in mice kept on a low-Mg^{2+} diet and in mouse DCT cells grown in low-Mg^{2+}-containing media.[15] Moreover, when expressed in *Xenopus laevis* oocytes, CNNM2 induced the transport of a range of divalent cations, including Mg^{2+} but not Ca^{2+}.[15]

In the present study, we investigated *CNNM2* (MIM 607803) as a candidate gene for unresolved human Mg^{2+} wasting phenotypes and identified mutations in two unrelated families with dominant hypomagnesemia.

Subjects and Methods

Patients

Informed consent to participate in this study was obtained from the patients and their participating relatives. The procedures followed were in accordance with the standards of the medical ethics committee of each participating institution.

Family A

Details of the index patient and her father have been extensively described elsewhere.[16] In brief, in both individuals (Figure 1A, left), severely lowered serum Mg^{2+} values were determined before oral Mg^{2+} supplementation was started (0.46 mmol/l and 0.51 mmol/l in father and daughter, respectively [normal 0.70–1.15 mmol/l]). For the father, a detailed urinary examination was performed prior to the start of Mg^{2+} supplementation. Ca^{2+} was found to be in the low to normal range 0.05–0.10 Ca^{2+}/creatinine molar ratio, normal 0.06–0.45) and his urinary Mg^{2+} excretion was in the normal range (0.1–0.2 Mg^{2+}/creatinine molar ratio, normal 0.2–0.3). In view of the low serum Mg^{2+} levels, normal urinary Mg^{2+} excretion suggests a renal defect in Mg^{2+} reabsorption. The age of onset of symptoms was variable among the two family members: onset was 15 years of age for the father, whereas the index patient was hospitalized for being symptomatic in the first two years of life.

Family B

The index patient in family B (Figure 1A, right) was admitted to the hospital at 16 years of age. He suffered from weakness of the limbs, vertigo, and headaches. Laboratory examination revealed a low serum Mg^{2+} of 0.36 mmol/l and a urinary Ca^{2+} excretion of 2.7 mmol/24 hr, which is in the low to normal range (normal 2.5–8.0). All other measured values were normal (including serum: Na^{+}, 143 mmol/l [normal 136–146]; K^{+}, 4.5 mmol/l [normal 3.5–5.1]; Ca^{2+}, 2.47 mmol/l [normal 2.15–2.60]; urine: urea 271 mmol/24 hr [normal 150–500]; creatinine, 10.1 mmol/24 hr [normal 4.5–18]; Na^{+}, 125 mmol/24 hr [normal 40–220]; K^{+}, 40 mmol/24 hr [normal 25–125]; Cl^{-}, 142 mmol/24 hr [normal

110–250]; Mg^{2+}, 6.7 mmol/24 hr [normal 2.5–8.5]). Again, the combination of normal urinary Mg^{2+} excretion and low serum Mg^{2+} levels points to a renal Mg^{2+} reabsorption defect. Only serum values were available for the mother. She did not display symptoms; however, her serum Mg^{2+} was found to be low (0.52 mmol/l). Ca^{2+} (2.5 mmol/l), PO_4^{3-} (1.19 mmol/l), alkaline phosphatase (1.51 μkat/l), and parathyroid hormone (123 pg/ml) were in the normal range. Although the index patient was supplemented with Mg^{2+}, after which a serum Mg^{2+} level of 0.61 mmol/l was reached, a complete normalization of serum Mg^{2+} was not observed. The index patient and his mother were lost for further follow-up studies.

Mutation Analysis

Genomic DNA from peripheral blood was isolated using standard methods. After previous exclusion of mutations in *FXYD2*, *EGF*, and *SLC12A3* (MIM 600968) (data not shown), individuals from a Dutch family (Family A, Figure 1A, I.1, II.3, and III.2) and a family from the Czech Republic (Family B, Figure 1A, I.2 and II.1) were tested for mutations in the coding region of *CNNM2* (NM_017649.3) by direct sequencing of amplified exonic PCR products. Primers were designed using Primer3 software.[17] Amplicons generated for sequencing included at least 80 nucleotides upstream and 30 nucleotides downstream of the exonic sequence to cover possible mutations in branch and splice sites. Primer sequences and PCR conditions are listed in Table S1 (available online). We checked for the absence of identified mutations in 202 and 214 ethnically matched control chromosomes in family A and family B, respectively.

Bioinformatics

We performed a multiple sequence alignment of the CNNM2 protein with its three human homologs and with six orthologs using ClustalW. For a prediction of the membrane topology, the following web services were used: Human Protein Atlas, TMHMM Server v. 2.0, and Consensus Prediction of Membrane Protein Topology. Protein signatures were determined using the InterPro database.

Antibody Generation

A guinea pig anti-CNNM2 polyclonal antibody directed against the CNNM2-specific peptide CGLNHSDSLSRSDRI, corresponding to amino acids 754–768 of both the human and mouse protein, was generated by Biogenes (Berlin, Germany). In brief, guinea pigs were injected on day 1 with 0.5 mg synthetic peptide conjugated with the carrier protein Limulus polyphemus hemocyanin, and preimmune serum was withdrawn. Subsequent boosts of 1 × 0.25 mg and 3 × 0.125 mg peptide were performed on days 14, 28, 56, and 84, followed by a final bleeding on day 98. The antibody response in the serum from the final bleeding was compared with antibody response from the preimmune serum from the same animal to ensure specificity (Figure S1).

Immunohistochemistry

Four percent (w/v) paraformaldehyde fixed and paraffin-embedded human kidney sections from healthy human kidneys were stained sequentially with the antibody against CNNM2 and an antibody against uromodulin/Tamm-Horsfall protein (UMOD [MIM 191845]), parvalbumin (PVALB [MIM 168890]), or the thiazide-sensitive Na^+-Cl^- cotransporter (NCC) (Figure 2). In short, after deparaffinization and rehydration, sections were blocked with 3% (v/v) goat serum for 20 min. After blocking, sections were incubated for 1 hr with guinea pig anti-CNNM2 antibody (1:100) in PBS/3% (w/v) BSA. After washing, the secondary antibodies Alexa Fluor 488 or 633 goat anti-guinea pig IgG (Invitrogen, Belgium, 1:200) in PBS/3% (v/v) goat serum were applied for 1 hr. Sections were washed and blocked for 20 min with rabbit serum. After blocking, sections were incubated for 1 hr with sheep anti-UMOD (Meridian Life Sciences, 1:400), goat anti-PVALB (Santa Cruz, 1:200), or sheep anti-T58-NCC (purchased from the University of Dundee, UK, 1:100) in PBS/3% (w/v) BSA. After washing, appropriate Alexa Fluor 488 or 633 conjugated secondary antibodies (Invitrogen, 1:200) in PBS/3% (v/v) rabbit serum were applied for 1 hr. Sections were mounted in ProLong Gold Antifade reagent (Invitrogen) and viewed under a Zeiss LSM 510 Meta confocal microscope (Zeiss, Belgium). The images were analyzed with ImageJ software.

Four-micrometer-thick sections of 4% (w/v) paraformaldehyde fixed and paraffin-embedded kidneys of C57BL/6 mice (Figure S2) were similarly processed except that antibodies against CNNM2 and the nephron markers were not applied sequentially. Here, the primary antibodies were guinea pig anti-CNNM2 (1:100), rabbit anti-UMOD (Biomedical Technologies, 1:250), and rabbit anti-NCC (a kind gift from Dr. D.H. Ellison, 1:200). The secondary antibodies were Alexa Fluor 488 goat anti-guinea pig IgG and Alexa Fluor 594 goat anti-rabbit IgG (both Invitrogen, 1:500). Fluorescence microscopy of these sections was performed with a Leica DM IRE2 inverted microscope, and images were taken with Openlab software.

Cloning

To obtain CNNM2 expression constructs, we used the full-length murine *Cnnm2* cDNA, RIKEN FANTOM clone 6330543C15, GenBank accession number AK032006.1. Compared to RefSeq NM_033569.3, it contained two errors in its coding region (c.560A>G [p.Lys187Arg] and c.1329delC [p.Lys444ArgfsX6], where +1 is the A of the translation initiation codon). These were corrected using the QuikChange site-directed mutagenesis kit (Stratagene) according to the manufacturer's protocols. This resulted in clone pFLCI-mCnnm2WT. To obtain a construct with the missense mutation c.1703C>T (p.Thr568Ile) found in family B, we performed another mutagenesis round, resulting in clone pFLCI-mCnnm2Mut.

For the generation of C-terminally HA-tagged eukaryotic expression constructs, the open reading frames of the two pFLCI clones were amplified using Phusion polymerase (Finnzymes) and primers For1 and Rev1 (Table S2) to introduce an in-frame HA tag before the stop codon and KpnI and XbaI restriction sites. The amplicons were cloned into pGEM-T easy (Promega) and subcloned into the pcDNA3 expression vector (Invitrogen) via the KpnI and XbaI restriction sites.

For cloning of wild-type and p.Thr568Ile mutant CNNM2 in the bicistronic-enhanced GFP expression vector pCINeo-IRES-GFP[18] and introduction of an in-frame C-terminal HA tag, the open reading frames of the two pFLCI clones were amplified using primers For2 and Rev2 (Table S2) and cloned using NheI and XhoI restriction sites.

All clones were sequence verified for the complete CNNM2 coding region.

Immunocytochemistry

Mouse distal convoluted tubule (mDCT) cells were kindly provided by Dr. P.A. Friedman (University of Pittsburgh School of Medicine, Pittsburgh, PA). The isolation and functional characterization of these cells has been described previously.[19,20] The

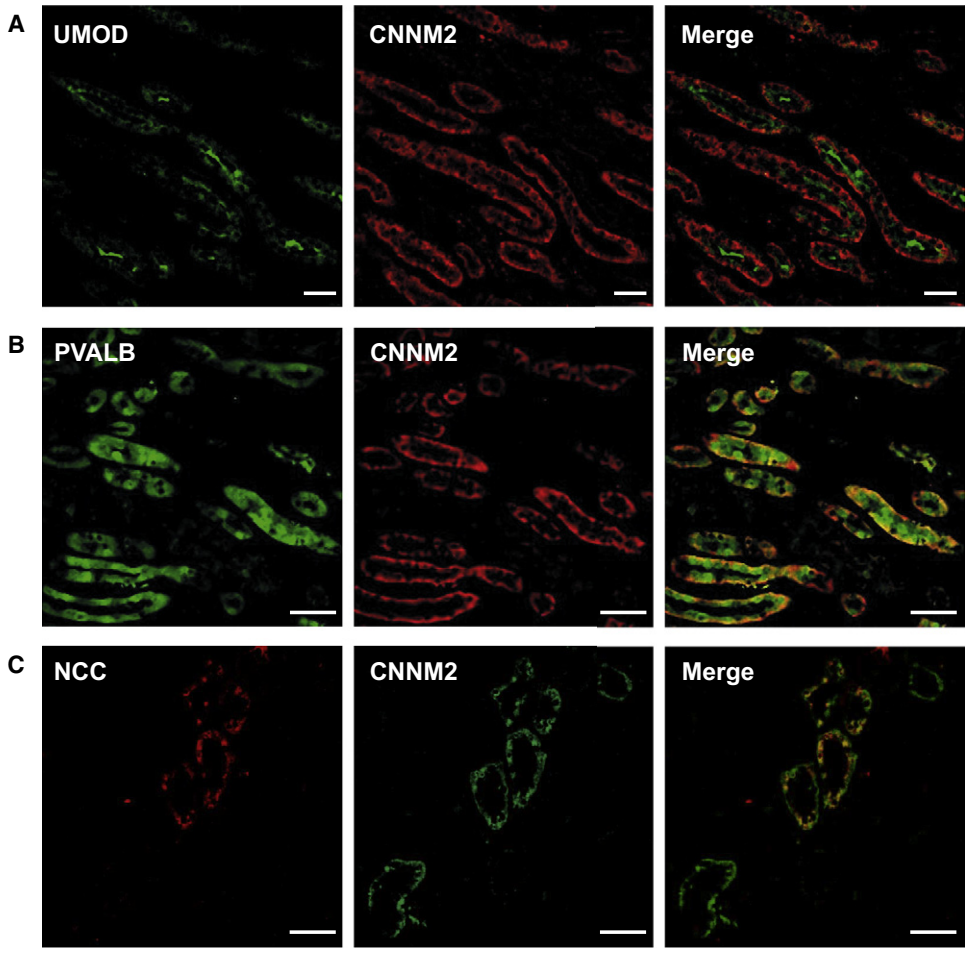

Figure 2. Immunohistochemical Analysis of CNNM2 in Human Kidney
(A) Staining of a human kidney section with antibodies against UMOD (left, in green) and CNNM2 (middle, in red). The merged image on the right shows codistribution of UMOD and CNNM2 in identical nephron segments, indicating basolateral subcellular staining of CNNM2 in the TAL. The scale bars represent 50 μm.
(B) Immunostaining for PVALB (left, in green) and CNNM2 (middle, in red) of a human kidney section. The merged image on the right indicates codistribution of PVALB in the DCT with basolaterally localized CNNM2. The scale bars represent 50 μm.
(C) A human kidney section stained with antibodies against NCC (left, in red) and CNNM2 (middle, in green). Merging the images as shown on the right shows that all NCC positive tubules are positive for CNNM2, indicating the presence of CNNM2 in the DCT. The scale bars represent 50 μm.

cells were grown in DMEM/Ham's F-12 media (Lonza, Verviers, Belgium), supplemented with 5% (v/v) fetal bovine serum (Lonza), 2 mM L-glutamine, 50 U/ml penicillin, and 50 μg/ml streptomycin in a humidified environment of 5% (v/v) CO_2 at 37°C. Where indicated, subconfluent mDCT cells were cultured in Mg^{2+}- or Ca^{2+}-free media (HyClone DMEM/High glucose, Thermo Scientific) for 18 hr. Other constituents of the Mg^{2+}- or Ca^{2+}-free media were similar to those in the complete media. Cell passages 20–35 were used in the present study. mDCT cells were fixed with 4% (w/v) paraformaldehyde, permeabilized (0.2% [v/v] Triton X-100 in PBS), and blocked (3% [v/v] goat serum in PBS). The cells were incubated with the primary antibody against CNNM2 (1:100 in PBS/2% [w/v] BSA) for 1 hr, followed by an incubation for 45 min with Alexa Fluor 488-conjugated secondary anti-guinea pig IgG antibodies (Invitrogen, 1:200). The cells were mounted in ProLong Gold antifade reagent containing DAPI (Invitrogen). Cells were viewed under a Zeiss LSM 510 Meta confocal microscope (Zeiss, Belgium). The images were analyzed with ImageJ software.

Aliquots of 1×10^6 MDCK-C7 cells[21] were transfected with 2 μg of pcDNA3 constructs expressing C-terminally HA-tagged wild-type or p.Thr568Ile mutant CNNM2 with the Amaxa Nucleofactor Kit T (program U-023, Lonza, Cologne, Germany). Cells were directly seeded onto filter supports (Millicell PCF 0.4 μm pore size, effective area 0.6 cm^2, Millipore, Bedford, MA) and grown in MEM with Earle's salts (PAA Laboratories, Pasching, Austria), supplemented with 10% (v/v) fetal bovine serum, 100 U/ml penicillin, and 100 μg/ml streptomycin (PAA) at 37°C in a humidified 5% (v/v) CO_2 atmosphere for 12 to 36 hr. Cells were rinsed in PBS, fixed in methanol (−20°C, 10 min), permeabilized (0.5% [v/v] Triton X-100 in PBS, 10 min), blocked (2% [v/v] goat serum in PBS), and incubated with mouse anti-HA (Cell Signaling Technology, 1:100) and rabbit anti-occludin (Invitrogen, 1:100) antibodies in blocking solution for 1 hr at 37°C, followed by incubation with cy2-conjugated goat-anti-mouse and cy5-conjugated goat anti-rabbit antibodies (both Jackson ImmunoResearch, 1:500) and 1 μM DAPI (Roche) for 45 min at 37°C. Filter supports with immunostained cells were mounted in ProTaqs Mount Fluor

(Biocyc, Germany) for investigation under a Zeiss LSM 510 META confocal microscope (Jena, Germany). Images and videos were generated with LSM Image Browser software.

Quantitative Real-Time PCR

mDCT cells were grown under control conditions or low-Mg^{2+} or low-Ca^{2+} conditions for 18 hr as described above. Total RNA was extracted via the RNAqueous-Micro kit (Ambion) according to the manufacturer's protocol. Quality and concentration of the isolated RNA preparations were analyzed using the 2100 Bioanalyzer (RNA Pico chip, Agilent Technologies, Palo Alto, CA). One microgram of RNA was used for reverse transcription using the iScript cDNA Synthesis Kit (Bio-Rad). Real-time PCR primers (Table S3) were designed using Primer3 software.[17] PCR reactions were performed on a CFX96™ Real-Time PCR Detection System (Bio-Rad Laboratories, Hercules, CA). Reactions were done in duplicate using iQ™ SYBR Green Supermix (Bio-Rad) with primer concentrations of 100 nM in 20 μl reactions. PCR conditions were 95°C for 3 min followed by 40 cycles of 15 s at 95°C and 30 s at 60°C. A single PCR product accumulation was detected and the PCR products were checked by sequencing. Relative changes in target gene/*Gapdh* mRNA ratio were determined by the formula $2^{-\Delta\Delta Ct}$.[22] Comparable results were obtained when *Actb* was used as the reference gene (data not shown).

Electrophysiology

Human embryonic kidney (HEK) 293 cells seeded in 12-well plates were transfected, via Lipofectamine 2000, (Invitrogen) with 1 μg of pCINeo-IRES-GFP constructs encoding C-terminally HA-tagged wild-type or p.Thr568Ile mutant CNNM2. After 12 hr, transfected cells were plated at low density on glass coverslips coated with fibronectin (Roche). Cells were maintained at 37°C in DMEM and supplemented with 10% (v/v) fetal bovine serum, essential amino acids, and L-glutamine in 5% (v/v) CO_2 atmosphere. Patch-clamp experiments were performed under the whole-cell configuration with an EPC-9 patch-clamp amplifier controlled by the Pulse software (HEKA Elektronik, Germany). Borosilicate patch pipettes had resistances between 3 and 4 MΩ after they were filled with the intracellular solutions. Series resistances (3–10 MΩ) were continuously monitored with the automatic capacitance compensation of Pulse software. All patch-clamp experiments were performed at room temperature (21°C). To study Na^+-dependent inward currents from wild-type and mutant CNNM2-expressing cells, we applied a repetitive voltage ramp protocol consisting of −120 to +80 mV over 450 ms duration every 2 s from a holding potential of 0 mV. The density current was obtained from the peak current at −110 mV and was normalized with the capacitance value of the cell obtained from the set-up. Extracellular solutions were (in mM) 80 Na^+-gluconate, 10 HEPES, 120 mannitol (pH 7.35 adjusted with Tris), and 80 Na^+-gluconate, 20 $MgSO_4$, 10 HEPES, 80 mannitol (pH 7.35 adjusted with Tris). The intracellular solution was (in mM): 120 N-methyl-D-glucamine (NMDG), 120 2-(N-morpholino)-ethanesulfonic acid hydrate (MES), 2 $MgSO_4$, 10 HEPES (pH 7.2 H_2SO_4). The analysis and display of patch-clamp data were performed by using Igor Pro software version 6.0 (WaveMetrics, Lake Oswego, OR, USA).

Cell Surface Biotinylation and Immunoblotting

HEK293 cells were transfected with pCINeo/IRES-GFP constructs expressing HA-tagged wild-type or p.Thr568Ile mutant CNNM2, as described above. After 48 hr, cells surfaces were biotinylated with sulfo-NHS-LC-LC-biotin (Pierce, Rockford, IL, USA). Cells were lysed with a Triton-containing lysis buffer, and 5% of the protein amount was collected as a total sample. Subsequently, the biotinylated proteins of the remaining 95% were precipitated with NeutrAvidin-agarose beads (Pierce, Rockford, IL, USA). We resolved total protein and plasma membrane fractions by SDS-PAGE and analyzed CNNM2 expression by immunoblot analysis with mouse anti-HA antibodies for the input and the plasma membrane fraction (Cell Signaling Technology). Probing blots with anti-β-actin antibodies (Sigma) confirmed equal loading and the absence of cytosolic proteins in the biotinylated fraction.

Statistics

Data are expressed as the mean ± standard error of the mean (SEM). Data in Figure 3A were analyzed with an unpaired Student's t test. Data in Figure 4C were analyzed with paired (0 versus 20 mM Mg^{2+}) and unpaired (wild-type versus mutant) Student's t tests. p values of less than 0.05 were considered significant.

Results

Mutations in *CNNM2* Cause Dominant Hypomagnesemia

Here, affected individuals of two unrelated families with dominant hypomagnesemia were tested for mutations in *CNNM2*. In both families, the index patient had severely lowered serum Mg^{2+} levels (0.51 mmol/l and 0.36 mmol/l in family A and B, respectively) in the absence of other electrolyte disturbances. Affected individuals in both families showed an inappropriately normal urinary Mg^{2+} excretion, demonstrating a defect in tubular reabsorption (details in Subjects and Methods).

Mutation screening of *CNNM2* (NM_017649.3) revealed a heterozygous 1 bp deletion, c.117delG in the index patient of family A, and a heterozygous missense mutation c.1703C>T in the index patient of family B (Figure 1A). In family A, the corresponding deletion was also detected in the father (II.3) but not in the grandfather (I.1) of the index patient. In family B, the mother (I.2) carried the same missense mutation as the index patient. Neither of the two mutations was found in more than 200 ethnically matched control chromosomes.

The 1 bp deletion c.117delG (p.Ile40SerfsX15) causes a frameshift and premature stop codon, leading to a truncated protein of 53 amino acids. The missense mutation c.1703C>T, causing a substitution of the threonine at position 568 with an isoleucine (p.Thr568Ile), is located in the most conserved region of CNNM2, termed ancient conserved domain (ACD) (Figure 1B).[23] A multiple sequence alignment of the CNNM2 protein with its three human homologs and with six orthologs down to the *Salmonella* bacterium (Figure 1C) shows that the threonine at position 568 is highly conserved.

One nonsynonymous SNP, c.113G>A (p.Arg38Gln), was detected in our patients. We confirmed it to be a SNP by testing control chromosomes (n = 214), where it was found seven times. Moreover, it was also listed in the NCBI database of genetic variation (rs76057237, dbSNP build 131).

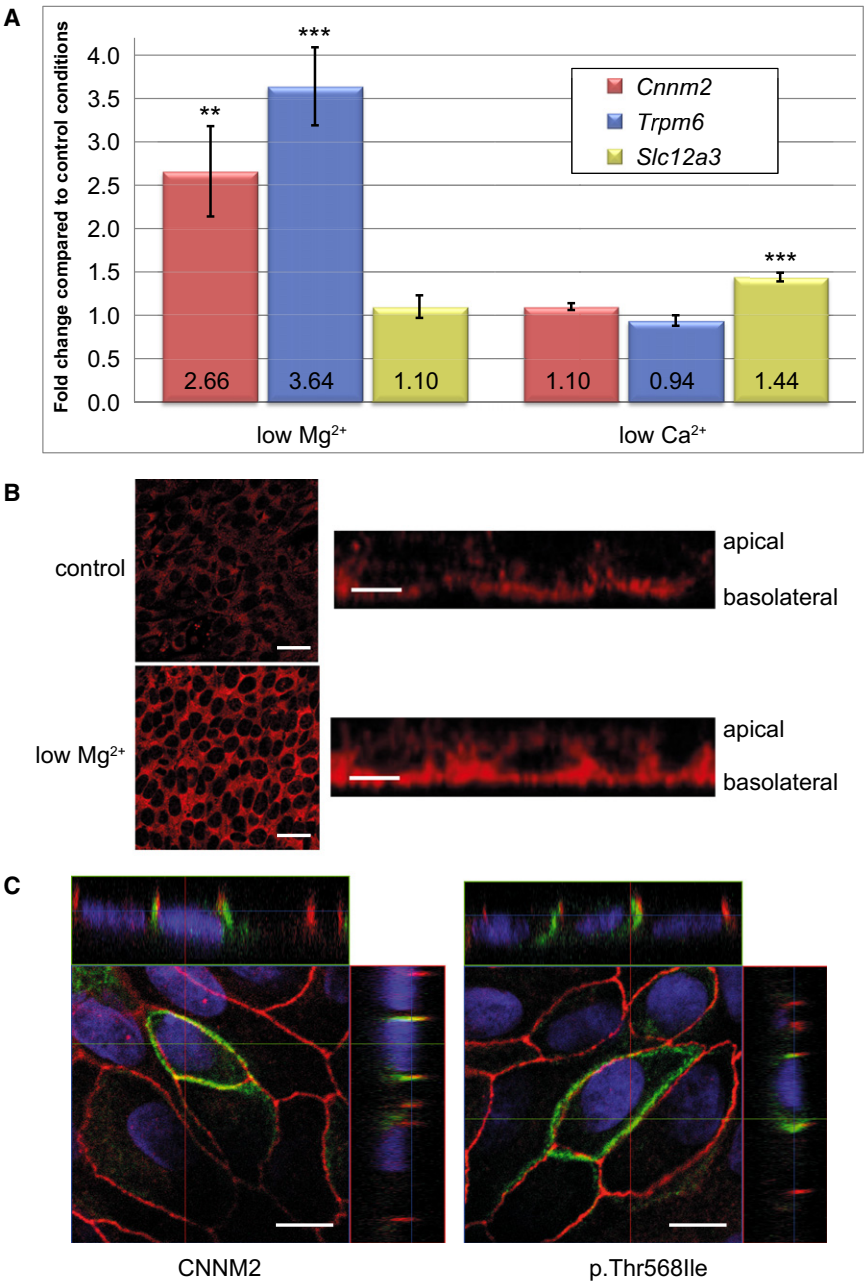

Figure 3. Response to Extracellular Mg^{2+} and Basolateral Localization of CNNM2 in Cultured Cells

(A) Modulation of *Cnnm2*, *Trpm6*, and *Slc12a3* mRNA levels under low-Mg^{2+} or low-Ca^{2+} conditions. mDCT cells showed increased expression levels of *Cnnm2* (in red) and *Trpm6* (in blue) after 18 hr growth under low-Mg^{2+} (left bars) but not under low-Ca^{2+} conditions (right bars) as determined by quantitative real-time PCR. The *Slc12a3* transcript (*Ncc*, in yellow) was used as a positive control for low-Ca^{2+} conditions. Expression levels are normalized to those of *Gapdh* and shown as fold change difference compared to control conditions. n = 6, data are shown as means ± SEM. **$p < 0.01$; ***$p < 0.001$ compared to normal culture conditions.

(B) Effect of low Mg^{2+} on endogenous CNNM2 protein levels in polarized mDCT cells as shown by immunolabeling with antibodies against CNNM2 (in red). After 18 hr growth under low-Mg^{2+} conditions, mDCT cells showed increased CNNM2 expression (bottom left) when compared to control conditions (top left) with identical recording settings. Predominant basolateral staining was observed in Z stacks for both control (top right) and low-Mg^{2+} conditions (bottom right). The scale bars represent 20 μm (left) and 5 μm (right).

(C) Confocal images of transiently transfected MDCK-C7 cells with wild-type (left) and p.Thr568Ile mutant (right) CNNM2-HA-tagged constructs. Cells were immunostained with antibodies against the HA tag (in green) and costained with antibodies against the tight junction protein occludin (in red) as a boundary marker between the apical and basolateral compartment. Nuclei were counterstained with DAPI (in blue). Wild-type and p.Thr568Ile mutant CNNM2 showed comparable localization to the (baso-) lateral membrane. The scale bars represent 10 μm.

CNNM2 Is Localized on the Basolateral Side of Mg^{2+}-Transporting Nephron Segments in Human and Mouse Kidney and Upregulated under Low-Mg^{2+} Conditions

In view of the low serum Mg^{2+} levels detected in both families, the inappropriately normal level of urinary Mg^{2+} excretion pointed to a renal defect in Mg^{2+} reabsorption. To determine the renal localization of CNNM2, we generated a polyclonal antibody against a CNNM2-specific peptide. Subsequent immunohistochemistry on human kidney sections revealed that CNNM2 is expressed in both the thick ascending limb (TAL) of Henle's loop (Figure 2A), as indicated by codistribution with uromodulin/Tamm-Horsfall protein, and DCT (Figures 2B and 2C), as shown by codistribution with parvalbumin and the thiazide-sensitive Na^{+}-Cl^{-} cotransporter (NCC).[24,25] We obtained similar results for mouse tissue sections by using antibodies against uromodulin and NCC as markers for TAL and DCT, respectively (Figure S2). The staining pattern for CNNM2 was consistently basolateral, as confirmed by codistribution but not colocalization with the apical uromodulin and NCC proteins.

Cnnm2 was originally identified as a Mg^{2+}-responsive gene by differential gene expression via microarray analysis of mouse distal convoluted tubule (mDCT) cells under control and low-Mg^{2+} conditions.[15] We grew mDCT cells under low-Mg^{2+}, low-Ca^{2+}, or control conditions to test whether this upregulation is specific for

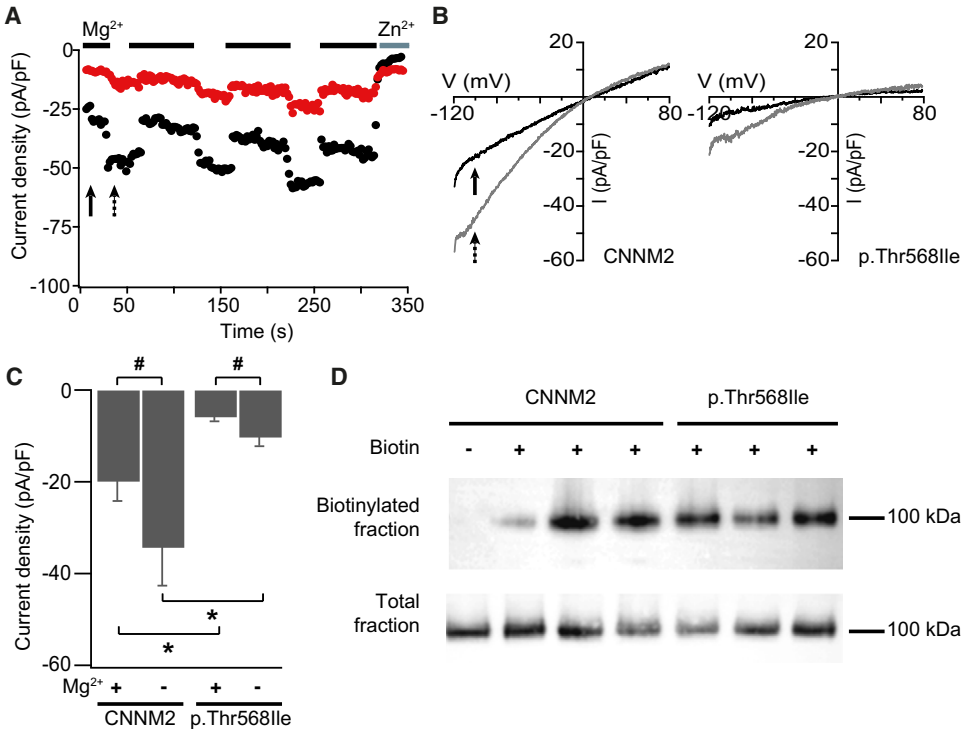

Figure 4. Electrophysiological Analysis of Wild-Type and p.Thr568Ile Mutant CNNM2

(A) Representative whole-cell current densities measured from HEK293 cells transiently transfected with expression constructs for wild-type CNNM2 (black dots) or p.Thr568Ile mutant CNNM2 (red dots). Current traces were recorded in a bath solution containing either 20 mM $MgSO_4$, (indicated by black bars above the graph) or 20 mM $ZnSO_4$ (gray bar) or in a Mg^{2+}- and Zn^{2+}-free bath solution (no bars). The solid and dotted arrows correspond to the time point of measurement in the presence or absence of extracellular Mg^{2+}, the results of which are shown in (B) and (C).

(B) Representative I-V relationship traces recorded either in the presence (solid arrow, traces in black) or absence of extracellular Mg^{2+} (dotted arrow, traces in gray). p.Thr568Ile mutant Na^{+}-evoked currents (right) were smaller under both perfusion conditions as compared to the wild-type CNNM2 protein (left).

(C) Histogram presenting averaged current densities at −110 mV obtained from wild-type (left) and p.Thr568Ile mutant CNNM2 (right) expressing HEK293 cells (n = 16 for both) in the presence and absence of 20 mM extracellular $MgSO_4$ (indicated by a + or a − symbol). Under both conditions, current amplitudes in cells expressing mutant CNNM2 were significantly smaller than those in cells expressing wild-type CNNM2. *$p < 0.05$, compared to wild-type CNNM2. #$p < 0.05$, compared to presence of 20 mM Mg^{2+}. The error bars denote SEM.

(D) Cell surface biotinylation of HEK293 cells expressing HA-tagged wild-type or p.Thr568Ile mutant CNNM2. A representative immunoblot shows comparable expression levels of mutant and wild-type protein on the membrane (upper blot) as well as in the total protein fraction (lower blot).

Mg^{2+} or could be induced by lowered Ca^{2+} as well,. Quantitative real-time PCR analysis of cDNA from these cells showed a significant upregulation of both *Cnnm2* and *Trpm6* transcripts (2.7- and 3.6-fold, respectively) under low Mg^{2+} when compared to control conditions, whereas low Ca^{2+} had no significant effect on *Cnnm2* or *Trpm6* mRNA levels (Figure 3A). *Slc12a3* (*Ncc*) expression has previously been shown to be upregulated under low-Ca^{2+} conditions and served as a positive control.[25]

To further substantiate the Mg^{2+}-responsive *Cnnm2* transcript levels and the basolateral localization of the protein, we cultured mDCT cells and stained the cells with the antibody against CNNM2 to detect endogenous expression of the protein. Under normal Mg^{2+} conditions, we were able to confirm the predominant basolateral localization of the CNNM2 protein (Figure 3B) that was increased in Mg^{2+}-deprived cells. Unfortunately, the antibody against CNNM2 has proven unsuitable for confirming this result by immunoblot analysis. In addition, we performed in vitro expression studies by transient transfection of polarized Madin-Darby canine kidney (MDCK)-C7 cells with a vector encoding HA-tagged wild-type CNNM2. Again, we detected localization of CNNM2 at the (baso-)lateral membrane (Figure 3C, left, and Movie S1). To test whether the missense mutation identified in family B affected the trafficking of the protein, we also expressed HA-tagged p.Thr568Ile mutant CNNM2 in MDCK-C7 cells (Figure 3C, right, and Movie S2). No obvious difference in subcellular localization was observed between mutant and wild-type protein.

Functional Characterization of CNNM2 and the p.Thr568Ile Mutant

Next, we investigated the functional characteristics of CNNM2 by using patch-clamp analysis in the whole-cell configuration of HEK293 cells that were transiently

transfected with constructs encoding HA-tagged wild-type CNNM2 or with mock DNA. Survival of HEK293 cells transfected with CNNM2 could be greatly improved by by inclusion of 20 mM $MgSO_4$ in the culture medium. Therefore, all cells were cultured and sealed in the presence of $MgSO_4$. Because Goytain and Quamme[15] observed Mg^{2+}-induced currents by CNNM2 expressed in *X. laevis* oocytes, we first applied a repetitive voltage ramps protocol in the presence of an increasing extracellular Mg^{2+} gradient as the sole charge carrier (2 to 40 mM). However, neither an inward nor an outward increase in current was observed in HEK293 cells expressing CNNM2 when these were compared to mock transfected cells (data not shown). Rather, in the presence of 80 mM extracellular Na^+-gluconate and 20 mM $MgSO_4$, a small Mg^{2+}-sensitive Na^+ current was observed at a holding potential of −110 mV, which was significantly and reversibly increased by removing extracellular $MgSO_4$ (Figure 4A, average values shown in Figure 4C). To disclose effects on the relatively small range currents (in the order of 20–100 pA/pF), we used Mg^{2+} concentrations of 0 and 20 mM $MgSO_4$, which are nonphysiological but not uncommon in electrophysiological experiments designed to reveal effects on such currents. The Mg^{2+}-sensitive Na^+ current could be completely blocked by 20 mM $ZnSO_4$. The I-V relationship (Figure 4B, left graph) shows a slightly inwardly rectifying current in the absence of extracellular Mg^{2+} (dotted arrow, gray trace). This current was reduced in the presence of extracellular Mg^{2+} (solid arrow, black trace). We did not observe a significant Mg^{2+}-sensitive Na^+ current in mock-transfected HEK293 cells (data not shown).

To characterize the effect of the p.Thr568Ile mutation on CNNM2 activity, we applied the same protocol as described above using a construct encoding p.Thr568Ile mutant CNNM2 in which we sequentially applied an extracellular solution that either contained 20 mM $MgSO_4$ or was Mg^{2+} free. Under these experimental conditions, a significant decrease in the basal inward Na^+ current, either in the presence (solid arrow) or absence (dotted arrow) of extracellular Mg^{2+}, was observed for the mutant (Figures 4A and 4B). Specifically, initial currents in the presence of 20 mM $MgSO_4$ were 19.5 ± 4.7 versus 5.5 ± 1.4 pA/pF (mean ± SEM, n = 16), compared to currents in the absence of extracellular Mg^{2+} that were 33.9 ± 8.8 versus 9.9 ± 2.4 pA/pF in wild-type and mutant CNNM2, respectively (Figure 4C). In both cases, application of Zn^{2+} produced a full block of the Na^+ current (Figure 4A).

Wild-type and mutant CNNM2 protein were expressed in similar amounts on the surface of the HEK293 cells as demonstrated by a cell surface biotinylation assay followed by immunoblot analysis (Figure 4D). Equal loading of the blots and absence of cytosolic proteins in the biotinylated fraction were checked by staining with antibodies against β-actin (Figure S3). Thus, our results show that mutation of the threonine at position 568 to isoleucine causes a significant decrease in CNNM2 activity present at the plasma membrane.

Discussion

Here, we have identified mutations in *CNNM2* in patients with dominant renal Mg^{2+} wasting. In the kidney, CNNM2 is predominantly localized on the basolateral side of TAL and DCT, the major Mg^{2+}-transporting nephron segments. The missense mutation found in our patients significantly impairs CNNM2 function as determined by electrophysiological analysis.

CNNM2 (cyclin M2) is a member of a family of four proteins, CNNM1–4 (MIM 607802; 607804; 607805).[23] The name results from a weak sequence similarity that is shared with the cyclin family, although a cyclin-like function has never been shown for CNNM1–4. Within the CNNM family, CNNM2 is the most conserved between man and mouse, having a 99.1% similarity and 97.8% identity on the protein level. CNNM2 has 875 amino acids and is predicted to have four to five transmembrane domains and an extracellular C terminus (Figure 1B). The CNNM proteins were previously called ACD proteins because of an evolutionarily conserved domain that shares high homology with the bacterial CorC protein.[23] Interestingly, this CorC protein, together with CorA, CorB, and CorD was found to be involved in Co^{2+} resistance and Mg^{2+} transport in *Salmonella typhimurium*.[26] A shared feature within the ACD is a tandem pair of cystathionine beta-synthase (CBS) domains (InterPro 000644) that are thought to form intramolecular dimeric structures.[27] CBS domains have been found in the ClC family of chloride channels and also in the bacterial Mg^{2+} transporter MgtE. Not surprising, the p.Thr568Ile substitution, located in the most conserved part of the ACD (Figure 1C), has a strong impact on CNNM2 function, as shown by the clearly diminished Mg^{2+}-sensitive Na^+ currents.

Perhaps as a result of the different expression systems used, our electrophysiology results on CNNM2 differ from previous results of Goytain and Quamme.[15] In mammalian HEK293 cells, we observed a Mg^{2+}-sensitive Na^+ current rather than the mediation of Mg^{2+} currents by CNNM2, as found upon expression in *X. laevis* oocytes. Despite this difference, our findings underline an emerging role for CNNM2 in renal Mg^{2+} handling. First, and similar to the results of Goytain and Quamme,[15] we showed that the *Cnnm2* transcript in mDCT cells is upregulated under conditions of Mg^{2+} deficiency, an effect not seen under low-Ca^{2+} conditions, suggesting a specific response to extracellular Mg^{2+} concentrations. By using our antibody against CNNM2, we were also able to show an elevated protein expression. Second, analogous to the results in mDCT cells, in *Cldn16* knockout mice, which display reduced serum Mg^{2+} levels, the expression of the *Cnnm2* transcript in the kidney was also shown to be increased.[14] Third, it has been described that in *Salmonella*, triple disruptant for the Mg^{2+} transporter genes *MgtA*, *MgtB*, and *CorA*, CNNM2 was able to partly complement the Mg^{2+}-dependent growth deficiency,[28] again suggesting an involvement of CNNM2 in Mg^{2+} transport. Finally, our

genetic findings that mutations in *CNNM2* cause dominant hypomagnesemia in humans are in line with the results of a recent genome-wide association study showing common variants in *CNNM2* to be associated with serum Mg^{2+} concentrations.[29] In this study, six loci, including *TRPM6*, were found influencing serum Mg^{2+}. In a secondary screen, the genome-wide association study also identified common variants in *CNNM2* and other members of the *CNNM* gene family.

In the families with dominant Mg^{2+} wasting presented here, we found two different types of mutation. In family A, we found an early frameshift, leading to a truncated protein of only 53 amino acids. In family B, we identified a substitution of a highly conserved amino acid that significantly impairs the function of the protein. Still, the affected individuals of both families display a nearly identical phenotype. Although this suggests to us that a reduced amount of functional protein may cause the disorder, the low number of patients does not allow us to make definite genotype-phenotype correlations, and we cannot rule out a dominant-negative effect. Future identification and analysis of additional families with mutations in *CNNM2* will help to clarify this point.

The biochemical findings between index patients and affected parents do not show marked differences. Notably, the serum Mg^{2+} levels in both index patients and affected parents are in the same decreased range. What is remarkable, however, is the variability in the age of clinical (symptomatic) onset of the disease. In family A, the onset of the disease in the index patient was at two years of age, in her father it was at 15 years of age; in family B, the affected mother did not show any symptoms at all. This intrafamiliar variability in age of onset and/or severity of symptoms is a well-known phenomenon for dominant diseases. For example, this was also observed for other dominant hypomagnesemia disorders, such as the families with an *FXYD2* mutation.[9,30] The mechanism(s) underlying this phenomenon have not yet been elucidated, but it is likely that genetic modifying factors and/or environmental factors are involved. At present these putative genetic and environmental predisposing risk factors are completely unknown.

Because CNNM2 expression is not restricted to the kidney (gene expression was reported to be ubiquitous and the highest levels were in kidney and brain),[15,23,31] we cannot exclude a contribution of other tissues to the observed hypomagnesemia in our patients. Importantly, however, the most prominent phenotype consists of a renal defect in Mg^{2+} reabsorption, as shown by the inability of the kidney to reduce urinary Mg^{2+} excretion under low serum Mg^{2+} conditions. A tissue-specific phenotype was also observed for patients with mutations in *CNNM4*, a gene that is ubiquitously expressed as well.[23,31] In this case, mutations lead to Jalili syndrome (MIM 217080), which features a phenotype restricted to the teeth (amelogenesis imperfecta) and eyes (cone-rod dystrophy).[32,33] We hypothesize that a reduction in the amount of functional CNNM2 in our patients will be most noticeable in the renal epithelia that reabsorb high amounts of Mg^{2+}.

In human and mouse kidney, we observed predominant CNNM2 expression in both TAL and DCT, the two consecutive nephron segments primarily responsible for Mg^{2+} reabsorption.[1] The DCT has been shown to be the nephron segment controlling final plasma Mg^{2+} concentrations, as exemplified by the DCT-specific expression of the Mg^{2+} channel TRPM6, the apical entry pathway for active Mg^{2+} transport.[13] CNNM2 expression in this segment is in line with a putative role in active Mg^{2+} reabsorption. In fact, as reviewed by Glaudemans et al.,[34] all proteins involved in primary familial hypomagnesemia identified to date, including TRPM6, Kv1.1, EGF, and the Na^+/K^+-ATPase γ-subunit, show codistribution in this nephron segment.

Surprisingly, we also found high levels of CNNM2 expression in TAL. This latter nephron segment has been reported to be responsible for up to ~70% of Mg^{2+} reabsorption, via passive, paracellular transport.[1] The high expression levels of CNNM2 in this nephron segment might either indicate a role of CNNM2 in affecting paracellular Mg^{2+} reabsorption pathways or rekindle the debate about the existence of an active Mg^{2+} reabsorption component in (cortical) TAL, as reviewed by Quamme.[35]

Both in TAL and DCT, CNNM2 was found at the basolateral side of the epithelium, and this basolateral localization was confirmed for endogenous CNNM2 in mDCT cells. We showed that the localization of CNNM2 on the basolateral membrane was unchanged for the p.Thr568Ile mutant when CNNM2 was transiently expressed in polarized MDCK-C7 cells. Thus, we concluded that the missense mutation does not influence basolateral sorting of CNNM2 in this renal cell line.

For decades, biochemical studies have predicted that an active extrusion mechanism in the transcellular transport of Mg^{2+} must exist, either via a Mg^{2+} pump or a Na^+/Mg^{2+} exchanger.[36] However, the molecular identity of such a transporter remains elusive. Although the finding of CNNM2 at the basolateral membrane could suggest an involvement in direct basolateral Mg^{2+} extrusion, the Mg^{2+} sensitivity of the Na^+ currents suggests that, in mammalian cells, CNNM2 might contribute to a Mg^{2+}-sensing mechanism rather than transporting Mg^{2+} itself. The tandem pair of CBS domains located in the highly conserved ACD might be directly involved in such a Mg^{2+}-sensing mechanism. This might be comparable to the Mg^{2+}-sensing mechanism of the bacterial Mg^{2+} transporter MgtE, for which the crystal structure was recently solved[37] and in which the CBS domains might play an important role in Mg^{2+}-sensing.[38]

In conclusion, we identified mutations in *CNNM2* associated with dominant hypomagnesemia by using a candidate gene approach. Future elucidation of the exact mechanism by which the basolaterally localized CNNM2 protein regulates renal Mg^{2+} reabsorption will add

fundamental insights to our understanding of kidney function and potentially lead to new therapeutic options.

Supplemental Data

Supplemental Data include three figures, three tables, and two movies and can be found with this article online at http://www.cell.com/AJHG/.

Acknowledgments

The authors are grateful to the members of the affected families for their participation in this study. We thank D.H. Ellison and P.A. Friedman for providing the anti-NCC antibody and the mDCT cells, respectively. We also thank F. van Zeeland for her excellent technical support. This work was supported by grants from the European Community, FP7 (EUNEFRON 201590) to C.A.W., O.D., N.V.A.M.K., I.C.M. and D.M., and the Deutsche Forschungsgemeinschaft (DFG FOR721) to D.G. and D.M. In addition, O.D. was financially supported by the Belgian agencies Fonds National de la Recherche Scientifique and Fonds de la Recherche Scientifique Médicale, the Fondation Alphonse and Jean Forton, a Concerted Research Action (10/15-029), an Interuniversity Attraction Pole (IUAP P6/05), and the programme d'excellence Marshall DIANE convention from the Région Wallonne, Belgium (Communauté Française de Belgique). C.A.W. was further supported by the Swiss National Science Foundation (3100A0-122217). R.J.B. and J.G.H. were supported by grants of the Netherlands Organization for Scientific Research (ZonMw 9120.6110; ZonMw 9120.8026; NWO ALW 818.02.001) and a European Young Investigator award (EURYI) 2006.

Received: December 24, 2010
Revised: February 14, 2011
Accepted: February 17, 2011
Published online: March 10, 2011

Web Resources

The URLs for data provided herein are as follows:

ClustalW, http://www.ebi.ac.uk/Tools/clustalw2
Consensus Prediction of Membrane Protein Topology, http://topcons.net
dbSNP, http://www.ncbi.nlm.nih.gov/SNP/
Human Protein Atlas, http://www.proteinatlas.org
Interpro Database, http://www.ebi.ac.uk/interpro
Online Mendelian Inheritance in Man (OMIM), http://www.ncbi.nlm.nih.gov/omim/
Primer3, http://frodo.wi.mit.edu/primer3
TMHMM Server v. 2.0, http://www.cbs.dtu.dk/services/TMHMM/

References

1. Quamme, G.A. (1997). Renal magnesium handling: New insights in understanding old problems. Kidney Int. *52*, 1180–1195.
2. Simon, D.B., Lu, Y., Choate, K.A., Velazquez, H., Al-Sabban, E., Praga, M., Casari, G., Bettinelli, A., Colussi, G., Rodriguez-Soriano, J., et al. (1999). Paracellin-1, a renal tight junction protein required for paracellular Mg2+ resorption. Science *285*, 103–106.
3. Konrad, M., Schaller, A., Seelow, D., Pandey, A.V., Waldegger, S., Lesslauer, A., Vitzthum, H., Suzuki, Y., Luk, J.M., Becker, C., et al. (2006). Mutations in the tight-junction gene claudin 19 (CLDN19) are associated with renal magnesium wasting, renal failure, and severe ocular involvement. Am. J. Hum. Genet. *79*, 949–957.
4. Hou, J., Paul, D.L., and Goodenough, D.A. (2005). Paracellin-1 and the modulation of ion selectivity of tight junctions. J. Cell Sci. *118*, 5109–5118.
5. Hou, J., Renigunta, A., Konrad, M., Gomes, A.S., Schneeberger, E.E., Paul, D.L., Waldegger, S., and Goodenough, D.A. (2008). Claudin-16 and claudin-19 interact and form a cation-selective tight junction complex. J. Clin. Invest. *118*, 619–628.
6. Günzel, D., Amasheh, S., Pfaffenbach, S., Richter, J.F., Kausalya, P.J., Hunziker, W., and Fromm, M. (2009). Claudin-16 affects transcellular Cl- secretion in MDCK cells. J. Physiol. *587*, 3777–3793.
7. Schlingmann, K.P., Weber, S., Peters, M., Niemann Nejsum, L., Vitzthum, H., Klingel, K., Kratz, M., Haddad, E., Ristoff, E., Dinour, D., et al. (2002). Hypomagnesemia with secondary hypocalcemia is caused by mutations in TRPM6, a new member of the TRPM gene family. Nat. Genet. *31*, 166–170.
8. Walder, R.Y., Landau, D., Meyer, P., Shalev, H., Tsolia, M., Borochowitz, Z., Boettger, M.B., Beck, G.E., Englehardt, R.K., Carmi, R., and Sheffield, V.C. (2002). Mutation of TRPM6 causes familial hypomagnesemia with secondary hypocalcemia. Nat. Genet. *31*, 171–174.
9. Meij, I.C., Koenderink, J.B., van Bokhoven, H., Assink, K.F., Groenestege, W.T., de Pont, J.J., Bindels, R.J., Monnens, L.A., van den Heuvel, L.P., and Knoers, N.V. (2000). Dominant isolated renal magnesium loss is caused by misrouting of the Na(+),K(+)-ATPase gamma-subunit. Nat. Genet. *26*, 265–266.
10. Groenestege, W.M., Thébault, S., van der Wijst, J., van den Berg, D., Janssen, R., Tejpar, S., van den Heuvel, L.P., van Cutsem, E., Hoenderop, J.G., Knoers, N.V., and Bindels, R.J. (2007). Impaired basolateral sorting of pro-EGF causes isolated recessive renal hypomagnesemia. J. Clin. Invest. *117*, 2260–2267.
11. Glaudemans, B., van der Wijst, J., Scola, R.H., Lorenzoni, P.J., Heister, A., van der Kemp, A.W., Knoers, N.V., Hoenderop, J.G., and Bindels, R.J. (2009). A missense mutation in the Kv1.1 voltage-gated potassium channel-encoding gene KCNA1 is linked to human autosomal dominant hypomagnesemia. J. Clin. Invest. *119*, 936–942.
12. Adalat, S., Woolf, A.S., Johnstone, K.A., Wirsing, A., Harries, L.W., Long, D.A., Hennekam, R.C., Ledermann, S.E., Rees, L., van't Hoff, W., et al. (2009). HNF1B mutations associate with hypomagnesemia and renal magnesium wasting. J. Am. Soc. Nephrol. *20*, 1123–1131.
13. Voets, T., Nilius, B., Hoefs, S., van der Kemp, A.W., Droogmans, G., Bindels, R.J., and Hoenderop, J.G. (2004). TRPM6 forms the Mg2+ influx channel involved in intestinal and renal Mg2+ absorption. J. Biol. Chem. *279*, 19–25.
14. Will, C., Breiderhoff, T., Thumfart, J., Stuiver, M., Kopplin, K., Sommer, K., Günzel, D., Querfeld, U., Meij, I.C., Shan, Q., et al. (2010). Targeted deletion of murine Cldn16 identifies extra- and intrarenal compensatory mechanisms of Ca2+ and Mg2+ wasting. Am. J. Physiol. Renal. Physiol. *298*, F1152–F1161.
15. Goytain, A., and Quamme, G.A. (2005). Functional characterization of ACDP2 (ancient conserved domain protein), a divalent metal transporter. Physiol. Genomics *22*, 382–389.

16. Meij, I.C., van den Heuvel, L.P., Hemmes, S., van der Vliet, W.A., Willems, J.L., Monnens, L.A., and Knoers, N.V. (2003). Exclusion of mutations in FXYD2, CLDN16 and SLC12A3 in two families with primary renal Mg2+ loss. Nephrol. Dial. Transplant. *18*, 512–516.
17. Rozen, S., and Skaletsky, H. (2000). Primer3 on the WWW for general users and for biologist programmers. Methods Mol. Biol. *132*, 365–386.
18. Trouet, D., Nilius, B., Voets, T., Droogmans, G., and Eggermont, J. (1997). Use of a bicistronic GFP-expression vector to characterise ion channels after transfection in mammalian cells. Pflugers Arch. *434*, 632–638.
19. Pizzonia, J.H., Gesek, F.A., Kennedy, S.M., Coutermarsh, B.A., Bacskai, B.J., and Friedman, P.A. (1991). Immunomagnetic separation, primary culture, and characterization of cortical thick ascending limb plus distal convoluted tubule cells from mouse kidney. In Vitro Cell. Dev. Biol. *27A*, 409–416.
20. Dai, L.J., Ritchie, G., Kerstan, D., Kang, H.S., Cole, D.E., and Quamme, G.A. (2001). Magnesium transport in the renal distal convoluted tubule. Physiol. Rev. *81*, 51–84.
21. Gekle, M., Wünsch, S., Oberleithner, H., and Silbernagl, S. (1994). Characterization of two MDCK-cell subtypes as a model system to study principal cell and intercalated cell properties. Pflugers Arch. *428*, 157–162.
22. Livak, K.J., and Schmittgen, T.D. (2001). Analysis of relative gene expression data using real-time quantitative PCR and the 2(-Delta Delta C(T)) Method. Methods *25*, 402–408.
23. Wang, C.Y., Shi, J.D., Yang, P., Kumar, P.G., Li, Q.Z., Run, Q.G., Su, Y.C., Scott, H.S., Kao, K.J., and She, J.X. (2003). Molecular cloning and characterization of a novel gene family of four ancient conserved domain proteins (ACDP). Gene *306*, 37–44.
24. Dahan, K., Devuyst, O., Smaers, M., Vertommen, D., Loute, G., Poux, J.M., Viron, B., Jacquot, C., Gagnadoux, M.F., Chauveau, D., et al. (2003). A cluster of mutations in the UMOD gene causes familial juvenile hyperuricemic nephropathy with abnormal expression of uromodulin. J. Am. Soc. Nephrol. *14*, 2883–2893.
25. Belge, H., Gailly, P., Schwaller, B., Loffing, J., Debaix, H., Riveira-Munoz, E., Beauwens, R., Devogelaer, J.P., Hoenderop, J.G., Bindels, R.J., and Devuyst, O. (2007). Renal expression of parvalbumin is critical for NaCl handling and response to diuretics. Proc. Natl. Acad. Sci. USA *104*, 14849–14854.
26. Gibson, M.M., Bagga, D.A., Miller, C.G., and Maguire, M.E. (1991). Magnesium transport in Salmonella typhimurium: The influence of new mutations conferring Co2+ resistance on the CorA Mg2+ transport system. Mol. Microbiol. *5*, 2753–2762.
27. Ignoul, S., and Eggermont, J. (2005). CBS domains: Structure, function, and pathology in human proteins. Am. J. Physiol. Cell Physiol. *289*, C1369–C1378.
28. Sponder, G., Svidova, S., Schweigel, M., Vormann, J., and Kolisek, M. (2010). Splice-variant 1 of the ancient domain protein 2 (ACDP2) complements the magnesium-deficient growth phenotype of Salmonella enterica sv. typhimurium strain MM281. Magnes. Res. *23*, 105–114.
29. Meyer, T.E., Verwoert, G.C., Hwang, S.J., Glazer, N.L., Smith, A.V., van Rooij, F.J., Ehret, G.B., Boerwinkle, E., Felix, J.F., Leak, T.S., et al; Genetic Factors for Osteoporosis Consortium; Meta Analysis of Glucose and Insulin Related Traits Consortium. (2010). Genome-wide association studies of serum magnesium, potassium, and sodium concentrations identify six Loci influencing serum magnesium levels. PLoS Genet. *6*, e1001045.
30. Meij, I.C., Saar, K., van den Heuvel, L.P., Nuernberg, G., Vollmer, M., Hildebrandt, F., Reis, A., Monnens, L.A., and Knoers, N.V. (1999). Hereditary isolated renal magnesium loss maps to chromosome 11q23. Am. J. Hum. Genet. *64*, 180–188.
31. Wang, C.Y., Yang, P., Shi, J.D., Purohit, S., Guo, D., An, H., Gu, J.G., Ling, J., Dong, Z., and She, J.X. (2004). Molecular cloning and characterization of the mouse Acdp gene family. BMC Genomics *5*, 7.
32. Polok, B., Escher, P., Ambresin, A., Chouery, E., Bolay, S., Meunier, I., Nan, F., Hamel, C., Munier, F.L., Thilo, B., et al. (2009). Mutations in CNNM4 cause recessive cone-rod dystrophy with amelogenesis imperfecta. Am. J. Hum. Genet. *84*, 259–265.
33. Parry, D.A., Mighell, A.J., El-Sayed, W., Shore, R.C., Jalili, I.K., Dollfus, H., Bloch-Zupan, A., Carlos, R., Carr, I.M., Downey, L.M., et al. (2009). Mutations in CNNM4 cause Jalili syndrome, consisting of autosomal-recessive cone-rod dystrophy and amelogenesis imperfecta. Am. J. Hum. Genet. *84*, 266–273.
34. Glaudemans, B., Knoers, N.V., Hoenderop, J.G., and Bindels, R.J. (2010). New molecular players facilitating Mg(2+) reabsorption in the distal convoluted tubule. Kidney Int. *77*, 17–22.
35. Quamme, G.A. (1989). Control of magnesium transport in the thick ascending limb. Am. J. Physiol. *256*, F197–F210.
36. Schweigel, M., and Martens, H. (2000). Magnesium transport in the gastrointestinal tract. Front. Biosci. *5*, D666–D677.
37. Hattori, M., Tanaka, Y., Fukai, S., Ishitani, R., and Nureki, O. (2007). Crystal structure of the MgtE Mg2+ transporter. Nature *448*, 1072–1075.
38. Ishitani, R., Sugita, Y., Dohmae, N., Furuya, N., Hattori, M., and Nureki, O. (2008). Mg2+-sensing mechanism of Mg2+ transporter MgtE probed by molecular dynamics study. Proc. Natl. Acad. Sci. USA *105*, 15393–15398.